ELSEVIER

Journal of Photochemistry and Photobiology A: Chemistry 105 (1997) 21–28

Journal of PHOTOCHEMISTRY AND PHOTOBIOLOGY A:CHEMISTRY

Photoinduced charge transfer processes of triplet benzophenone in acetonitrile

Markus von Raumer [a], Paul Suppan [a,*], Patrice Jacques [b]

[a] *Institute of Physical Chemistry of the University of Fribourg, Pérolles, CH-1700 Fribourg, Switzerland*

[b] *Laboratoire de Photochimie Générale, URA C.N.R.S. no. 431, ENSCMu 3, rue A. Werner 68093, Mulhouse, France*

Received 15 February 1996; accepted 11 December 1996

Abstract

Photoconductivity experiments of benzophenone in acetonitrile under nanosecond laser flash photolysis conditions result in the production of ions. Irradiation with laser energies of 3.5 eV and 4.7 eV reveals different ionization mechanisms. On excitation at 355 nm, the photocurrents are observed on the microsecond timescale. Energetic considerations and comparison of the experimental traces (variation in the ground state benzophenone concentration, laser pulse intensity and oxygen concentration) with simulations indicate that the ion-generating process at 355 nm is due to triplet–triplet annihilation. On excitation at 266 nm, a monomolecular biphotonic process is operative, resulting in the observation of photocurrents within the laser pulse. This difference is explained by the energy requirements of these processes, taking into account the dipole–induced dipole solvation interaction. © 1997 Elsevier Science S.A.

Keywords: Acetonitrile; Benzophenone; Photoinduced charge transfer

1. Introduction

The photoinduced ionization of a variety of aromatic molecules in acetonitrile (MeCN) has been reported to occur [1]. Laser flash photolysis experiments at 249 nm (4.98 eV) have revealed a monophotonic ionization mechanism. Other molecules, such as anthracene, show the same behaviour on excitation with laser pulses at 355 nm (3.5 eV) [2]. Laser excitation of perylene also leads to the formation of ions. In this case, the ion-generating mechanism has been attributed to self-quenching (SQ) and monophotonic ionization [3]. Recently, a study by Elisei et al. [4] showed that it was possible to create ions by the excitation of benzophenone (BP) in aqueous solution with 248 nm (5 eV) laser pulses. The main ion-forming process was assigned to two-photon ionization within the laser pulse. At very low laser intensities, ion generation on the microsecond timescale was observed. This second process was ascribed to triplet–triplet annihilation (TTA).

In this paper, the ionization processes of BP, excited at 355 nm (3.5 eV) or 266 nm (4.7 eV) in neat MeCN, are explored by applying the transient photoconductivity (TP) technique. Using MeCN as solvent, no pH effect disturbs the measurements, as is the case with water.

2. Experimental section

2.1. Photoconductivity

Photocurrents were recorded with a classical laser flash photolysis set-up. The excitation source was a nanosecond Nd:YAG laser (JK Lasers 2000) producing frequency-tripled 355 nm or frequency-quadrupled 266 nm pulses of 19 ns duration (pulse diameter, 6 mm). To monitor the laser pulse intensity, a fraction of the laser pulse was recorded with a calibrated photodiode. The main body of the TP cell (Fig. 1) was made of Voltalef®. The electrodes consisted of cylindrical pieces of platinum rod (diameter, 8 mm; contact with solution, 6 mm diameter) fitted into the main body. Standard connections joined the electrodes to the external wiring. The four optical windows consisted of 1 cm diameter, 5 mm thick quartz pieces, which were also fitted into the main body. One of the windows was fixed in a removable prolongation of the cell, where a standard taper ground glass joint round-bottomed flask could be fitted. With modified hexagon screws, electrodes and windows could be fitted very tightly, resulting in a vacuum proof system. The solution was deox-

* Corresponding author. Tel.: +41 026 300 8700; fax: +41 026 300 9737.

PII S1010-6030(96)04614-X

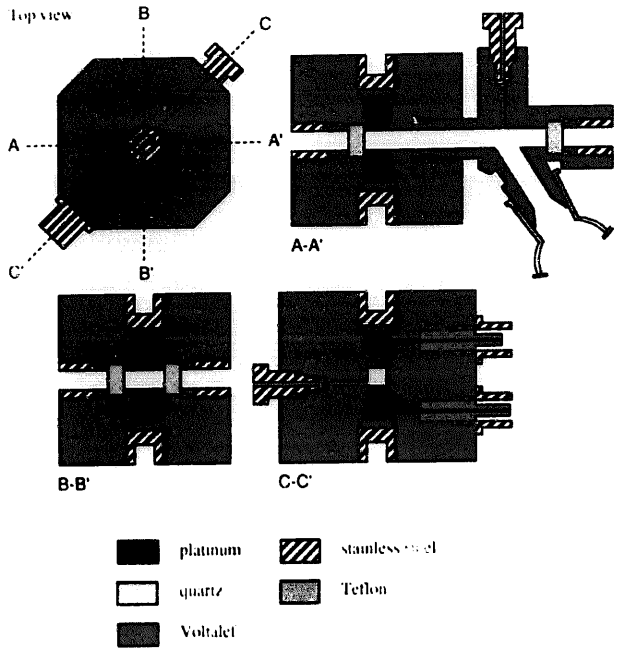

Fig. 1. Schematic view of the photocurrent cell.

ygenated either by argon bubbling or by the freeze–pump–thaw–shake (FPTS) technique. The electrodes were placed perpendicular to the windows allowing TP and transient absorption (TA) to be measured simultaneously. During the experiment, a grounded 2 mm thick aluminium shielding covered the whole cell. A d.c. voltage of 500 V was applied to one electrode and the current due to the presence of charged species in the sample was measured through an anodic load (50 Ω or 1 kΩ) on one channel of a digital storage 100 MHz oscilloscope (Gould 4074), interfaced with an Olivetti M240 computer. To prevent degradation of the sample, only single shot measurements were performed. Some signals of very low intensity may show a rather high noise level. The observed current can be related to the ion concentration by the following equation

$$i_{tot}(t) = i_+(t) + i_-(t) = \frac{n(t)q(\mu_+ + \mu_-)E}{d}$$

where $i(t)$ is the time-dependent observed current, E is the applied electric field (8.3×10^4 V m^{-1}), d is the electrode spacing (6×10^{-3} m), q is the charge of the particles, $n(t)$ is the time-dependent number of ions and $\mu_\pm$ is the mobility of the cation or anion. The mobility based on the Stokes–Einstein model is given by

$$\mu_\pm = \frac{q}{6\pi\eta r_\pm}$$

where η is the viscosity of the solvent (MeCN at 20 °C: 0.325×10^{-3} kg m^{-1} s^{-1} [5]) and $r_\pm$ is the radius of the charged species (4×10^{-10} m). An observed current of 1 μA results in an ion concentration of 3.36×10^{-8} M (volume of the cell is given by its dimensions, 1.7×10^{-4} dm^3). Normalization of the traces to unity is carried out by dividing them by their peak value. Such figures do not have any units for the ordinate.

2.2. Simulations

Simulations were performed with a home-written Fortran program using the DOPRI5 subroutine [6]. This subroutine allows the numerical solutions of first-order differential equations to be obtained using an explicit Runge–Kutta method of order five.

2.3. Compounds

The extinction coefficients in MeCN of ground state BP ($^1BP_0$) are approximately 100 M^{-1} cm^{-1} at 355 nm and 10 000 M^{-1} cm^{-1} at 266 nm. Triplet BP (^3BP) has an extinction coefficient of 6500 M^{-1} cm^{-1} at 525 nm [7]. BP (Aldrich Gold Label) was sublimated twice; MeCN (Fluka UV grade) was used without further purification.

3. Results

It is well known that BP yields quantitatively the lowest triplet state (n–π*) on UV irradiation. The deactivation pathways of ^3BP in benzene have been known for some time [8–10]. In addition to the radiative (phosphorescence) and non-radiative (intersystem crossing) pathways, which control the intrinsic lifetime of ^3BP, several other quenching mechanisms and photochemical reactions are known. In the absence of such reactions, the process determining the lifetime is generally SQ, where ^3BP is deactivated by $^1BP_0$ to yield two $^1BP_0$. Other processes which must be considered are impurity quenching (e.g. by oxygen) and TTA.

$$^3BP \rightarrow {}^1BP_0 \text{ (phosphorescence)} \quad (1a)$$

$$^3BP \rightarrow {}^1BP_0 \text{ (intersystem crossing)} \quad (1b)$$

$$^3BP + {}^1BP_0 \rightarrow {}^1BP_0 + {}^1BP_0 \text{ (SQ)} \quad (1c)$$

$$^3BP + {}^3BP \rightarrow {}^1BP^* + {}^1BP_0 \rightarrow {}^3BP + {}^1BP_0 \text{ (TTA)} \quad (1d)$$

$$^3BP + Q \rightarrow {}^1BP_0 + Q \text{ (impurity quenching)} \quad (1e)$$

The possible deactivation pathways in polar solvents are basically the same as the deactivation pathways in apolar solvents (Eqs. (1a)–(1e)), but ion-generating mechanisms must also be considered (Eqs. (2a)–(2d)). Direct ionization (via a two-photon process), electron transfer (ET) with the solvent, SQ and TTA may contribute to ionic deactivation processes.

$$^1BP_0(+2h\nu) \rightarrow BP^{\bullet+} + e^-_{solv}$$

(two-photon ionization) (2a)

$$^3BP + MeCN \rightarrow BP^{\bullet\pm} + MeCN^{\bullet\pm}$$

(ET with solvent) (2b)

$$^3BP + {}^1BP_0 \rightarrow BP^{\bullet-} + BP^{\bullet+} \text{ (SQ)} \quad (2c)$$

$$^3BP + {}^3BP \rightarrow BP^{\bullet-} + BP^{\bullet+} \text{ (TTA)} \quad (2d)$$

In all processes, the key role is held by the triplet concentration itself. The variation of the laser intensity directly influences the ^3BP concentration and will affect most of the processes given above. The alteration of the $^1BP_0$ concentration influences the SQ process as well as the absorbance (A) at the excitation wavelength, and thereby indirectly the triplet concentration. In addition, the deoxygenation efficiency affects the oxygen (O_2) content of the sample and, consequently, the ^3BP lifetime, since oxygen acts as a powerful quencher towards triplet states. The variation of the $^1BP_0$ concentration, laser intensity and O_2 concentration should, in principle, account for the ionization pathways.

The spectral identification of the charged transients by TA is not possible, because the $BP^{\bullet -}$ absorption at 710 nm is overlapped by the triplet absorption [11]; nothing is known about $BP^{\bullet +}$; neither the stability nor the absorption spectra are reported in the literature. The solvated electron, which could either be the acetonitrile radical anion $MeCN^{\bullet -}$ or the dimeric form $(MeCN)_2^{\bullet -}$, absorbs at 550 nm and 1450 nm [12]. The first wavelength is covered by the ^3BP absorbance and the latter lies beyond the detection range of our instrument.

Table 1
Variation of the initial experimental conditions

Figure	Laser pulse intensity	Parameters		Comment
		$[^1BP_0]$	$[O_2]$	
Fig. 2	Variable	Constant	Constant	
Fig. 3	Variable	Constant	Constant	Normalized
Fig. 4	Constant	Variable	Constant	Normalized
Fig. 5	Constant	Constant	Variable	Normalized

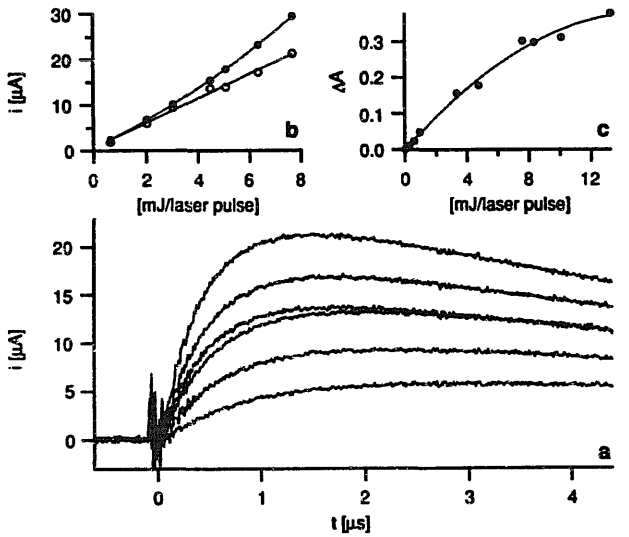

Fig. 2. (a) TP kinetics of BP ($[^1BP_0] = 1.1 \times 10^{-2}$ M, $A = 1.1$) in MeCN excited at 355 nm with different laser pulse intensities. (b) TP maxima plotted against the laser pulse intensity: uncorrected (○) and corrected for ^3BP saturation (●). (c) ^3BP absorbance at 525 nm plotted against the laser pulse intensity. Saturation of the absorbance is observed with increasing laser pulse intensity.

3.1. Excitation at 355 nm

3.1.1. Photocurrents

The variation of the initial experimental conditions is reported in Table 1.

Fig. 2 shows the photocurrents observed at different laser intensities for a $^1BP_0$ concentration equal to 1.1×10^{-2} M ($A = 1.1$). High laser pulse intensities (8 mJ per pulse) generate currents of 20 µA, a value which corresponds to an ion concentration of approximately 6.7×10^{-7} M. The ^3BP concentration at this excitation intensity corresponds to approximately 4×10^{-5} M. In Fig. 3, the normalized photocurrent traces at the same $^1BP_0$ concentration are shown at high and low laser intensity. In Fig. 4, the normalized photocurrent traces at constant laser pulse intensity but different $^1BP_0$ concentrations are shown.

The following conclusions are valid for 355 nm excitation.

1. No monomolecular two-photon ionization is observed (Eq. (2a)). This type of ionization would yield a current rise within the laser pulse.

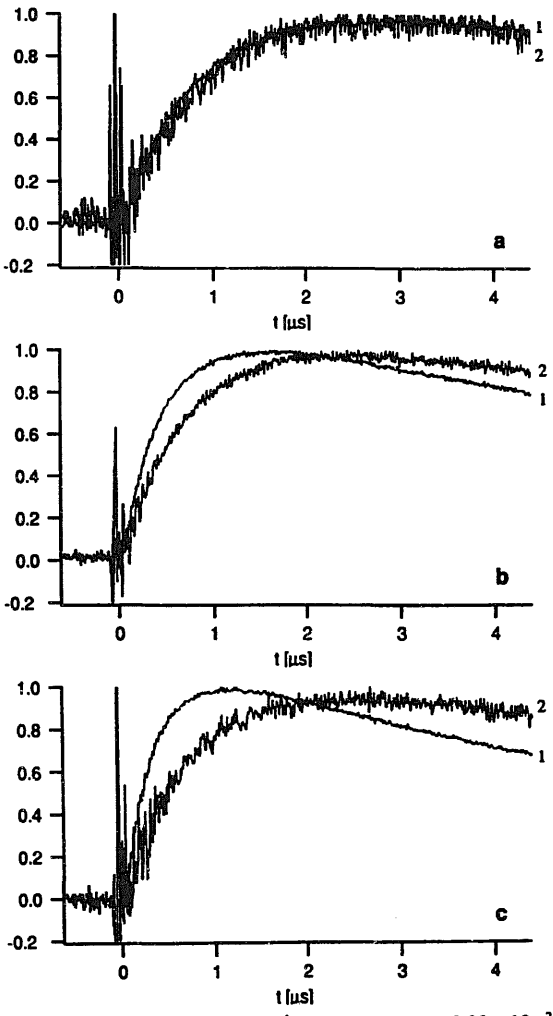

Fig. 3. Normalized TP kinetics. $[^1BP_0]$ (M): (a) 0.33×10^{-2}; (b) 1.1×10^{-2}; (c) 1.9×10^{-2}. Excited at 355 nm with high (approximately 7.5 mJ per pulse) (1) and low (approximately 2.5 mJ per pulse) (2) laser pulse intensities.

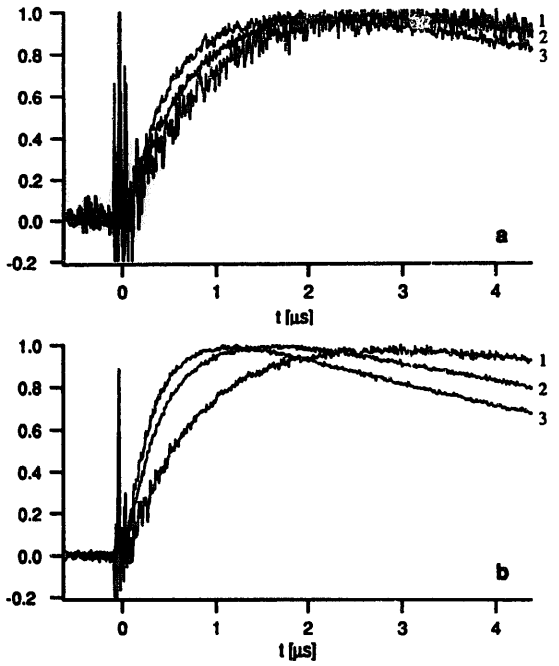

Fig. 4. Normalized TP kinetics excited at 355 nm with low (approximately 2.5 mJ per pulse) (a) and high (approximately 7.5 mJ per pulse) (b) laser pulse intensities. [$^1BP_0$] (M): 1, 0.33×10^{-2}; 2, 1.1×10^{-2}; 3, 1.9×10^{-2} M.

2. At the same laser pulse intensity, the steepness of the photocurrent rise increases with increasing $^1BP_0$ concentration of the sample.
3. At the same $^1BP_0$ concentration, the steepness of the photocurrent rise increases with increasing laser pulse intensity.

Fig. 5 shows the effect of molecular oxygen on the photocurrent rises.

A consideration of the energetics of the various ET processes should provide additional information on the operative ion-generating mechanism. The energy balance of an ET reaction is given by the well-known empirical Rehm–Weller equation, which uses the oxidation potential of the donor (E_{ox}(D)), the reduction potential of the acceptor (E_{red}(A)), the excited state energy (E_T) and a Coulomb term (C) to take into account the electrostatic interaction after ET

$$\Delta G_{ET} = E_{ox}(D) - E_{red}(A) - E_T + C$$

The classical expression for C, which considers point charges and the continuum solvent model, yields $C = -0.05$ eV in MeCN. We use the upper limit of -0.5 eV [13] to calculate the reaction free energies of the ET processes. These are reported in Table 2 for the postulated ET reactions.

ΔG_{ET} is endergonic for the SQ-ET mechanism and for the ET reaction with the solvent; these mechanisms are therefore unlikely to be important in these cases. The only exergonic reaction consists of TTA, which seems to be the ion-generating process of ^3BP in MeCN.

3.1.2. Simulations

By performing simulations of the possible deactivation pathways of ^3BP in MeCN, reproduction of the experimentally obtained photocurrents is possible. The variation of the initial parameters (concentrations) simulates the experimental conditions. Apart from the biphotonic monomolecular ionization and the reaction with the solvent, two ion-generating processes, SQ and TTA, are considered (see below).

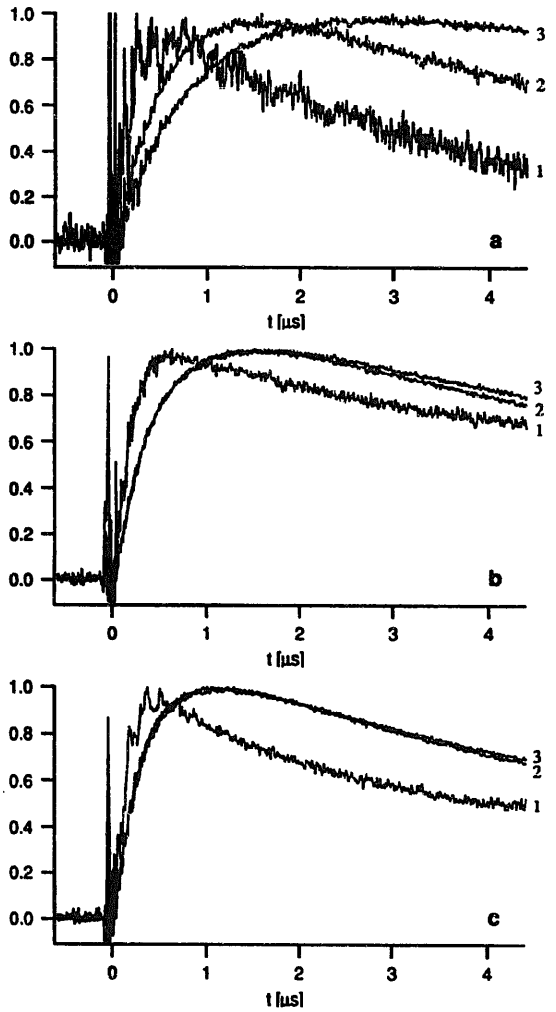

Fig. 5. Normalized TP kinetics excited at 355 nm (7.5 mJ per laser pulse). [$^1BP_0$] (M): (a) 0.33×10^{-2}; (b) 1.1×10^{-2}; (c) 1.9×10^{-2}; 1, not deoxygenated; 2, deoxygenated by bubbling argon through the sample for 20 min; 3, FPTS degassed.

$$^3BP \rightarrow {}^1BP_0 \quad (k_0) \tag{3a}$$

$$^3BP + {}^3BP \rightarrow {}^1BP^* + {}^1BP_0 \rightarrow {}^3BP + {}^1BP_0 \quad (k_{TT1}) \tag{3b1}$$

$$^3BP + {}^3BP \rightarrow BP^{\bullet-} + BP^{\bullet+} \quad (k_{TT2}) \tag{3b2}$$

$$^3BP + {}^1BP_0 \rightarrow {}^1BP_0 + {}^1BP_0 \quad (k_{SQ1}) \tag{3c1}$$

$$^3BP + {}^1BP_0 \rightarrow BP^{\bullet-} + BP^{\bullet+} \quad (k_{SQ2}) \tag{3c2}$$

$$^3BP + Q \rightarrow {}^1BP_0 + Q \quad (k_Q) \tag{3d}$$

Eq. (3a) describes the radiative and intersystem crossing decays, Eqs. (3b1) and (3b2) TTA through non-ionic and ionic pathways and Eqs. (3c1) and (3c2) SQ through non-ionic and ionic pathways. Eq. (3d) describes the possibility of deactivation by a quencher Q by a non-ionic pathway. Eqs. (3b1) and (3b2) can also be defined by a total rate constant

Table 2
Oxidation and reduction potentials of BP and MeCN. ΔG_{ET} for the different quenching mechanisms

Electrochemical potential (V) vs. SCE in MeCN			ET mechanism			ΔG^{a}_{ET} (eV)
Compound	E_{ox}	E_{red}		Donor	Acceptor	
BP	2.33[b]	−1.88[b]	SQ[c]	^{3}BP	^{1}BP$_0$	+0.71
MeCN	4.0[c]	−3.5[d]	SQ[e]	^{1}BP$_0$	^{3}BP	+0.71
			ET with solvent[f]	MeCN	^{3}BP	+2.33
				^{3}BP	MeCN	+2.38
			TTA[g]	^{3}BP	^{3}BP	−2.29

[a]Calculated using the Rehm–Weller equation ($E_T = 3$ eV, $C = -0.5$ eV).
[b]Ref. [14].
[c]This lower bound value can be assumed according to electrochemical data [15].
[d]Ref. [15].
[e]Eq. (2c).
[f]Eq. (2b).
[g]Eq. (2d).

$$k_{TT} = k_{TT1} + k_{TT2} = ak_{TT} + bk_{TT}$$

with

$$a + b = 1; \quad Pro_{TT} = b$$

We obtain

$$k_{TT} = (1 - Pro_{TT})k_{TT} + Pro_{TT}k_{TT}$$

The same also applies to k_{SQ} (Eqs. (3c1) and (3c2))

$$k_{SQ} = k_{SQ1} + k_{SQ2} = (1 - Pro_{SQ})k_{SQ} + Pro_{SQ}k_{SQ}$$

The weighting factors Pro_{TT} and Pro_{SQ} can adjust the relative importance of the ionic (Eqs. (3b2) and (3c2)) vs. non-ionic (Eqs. (3b1) and (3c1)) pathways. By taking into consideration only singly charged species and the overall electroneutrality of the sample, the same number of cations and anions can be assumed. Second-order recombination of the ions controlled by diffusion is described by a single rate constant k_{rec}. The differential equations can be written as

$$-\frac{d[T]}{dt} = (k_0 + 0.5(Pro_{TT} + 1)k_{TT}[T] + k_{SQ}[^1BP_0] + k_Q[Q])[T]$$

$$\frac{d[Cc]}{dt} + (Pro_{TT}k_{TT}[T] + 2Pro_{SQ}k_{SQ}[^1BP_0])[T] - k_{rec}[Cc]^2$$

where [T] is the ^{3}BP concentration and [Cc] is the charge carrier concentration. The appropriate choice of the initial concentrations of all species involved and a knowledge of the rate constants permits the simulation of the various pathways (Table 3).

SQ is constant for the same $^1BP_0$ concentration, independent of the laser pulse intensity. As SQ is a pseudo-first-order process, the laser intensity should have no influence on the steepness of the photocurrent rise if only the SQ mechanism (Eq. (3c2)) yields ions. However, a minor difference in the rise is to be expected, since non-ionic TTA must be considered (Eq. (3b1)); this is confirmed by the simulations (Fig. 6).

Since TTA is a second-order process, the laser pulse intensity is expected to play a role in the steepness of the photo-

Table 3
Parameters used for the simulations

Figure	Ion-generating process	Parameters[a]				
		$k_0 + k_Q[Q]$ (s^{-1})	Pro_{TT}	Pro_{SQ}	$[^1BP_0]$ (M)[b]	$[^3BP]$ (M)[b]
Fig. 6	SQ	0.2×10^6	0	1	0.005	1×10^{-6}–9×10^{-6}
Fig. 7	TTA	0.2×10^6	1	0	0.005	1×10^{-6}–9×10^{-6}
Fig. 8	SQ	0.2×10^6	0	1	0.001–0.050	Variable[c]
Fig. 9	TTA	0.2×10^6–2.2×10^6[d]	1	0	0.005	8×10^{-6}

[a]$k_{TT} = 1.8 \times 10^{10}$ M^{-1} s^{-1} [16,17], $k_{SQ} = 0.5 \times 10^6$ M^{-1} s^{-1} [10,16], $k_{rec} = 2.0 \times 10^{10}$ M^{-1} s^{-1} (diffusional limit).
[b]The initial concentrations are similar to the experimental conditions.
[c]The initial triplet concentration was adapted to the percentage of light absorbed by the sample, taking a value of 8×10^{-6} M at $[^1BP_0] = 0.005$ M.
[d][Q] varies from 9.5×10^{-6} M up to 1.095×10^{-4} M ($k_0 = 1 \times 10^{-4}$ s^{-1} and $k_Q = 2.0 \times 10^{10}$ M^{-1} s^{-1} (diffusional limit)).

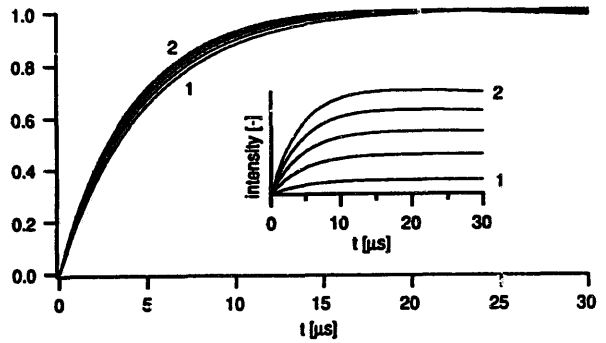

Fig. 6. Normalized and non-normalized (inset) simulated TP kinetics; only SQ is the ion-forming process. The following values were taken: $k_0+k_Q[Q]=0.2\times10^6\ s^{-1}$, $k_{TT}=1.8\times10^{10}\ M^{-1}\ s^{-1}$, $k_{SQ}=0.5\times10^6\ M^{-1}\ s^{-1}$, $k_{rec}=2.0\times10^{10}\ M^{-1}\ s^{-1}$, $Pro_{TT}=0$, $Pro_{SQ}=1$, $[^1BP_0]=0.005$ M. The initial triplet concentration [T] was varied from 1×10^{-6} M (1) up to 9×10^{-6} M (2).

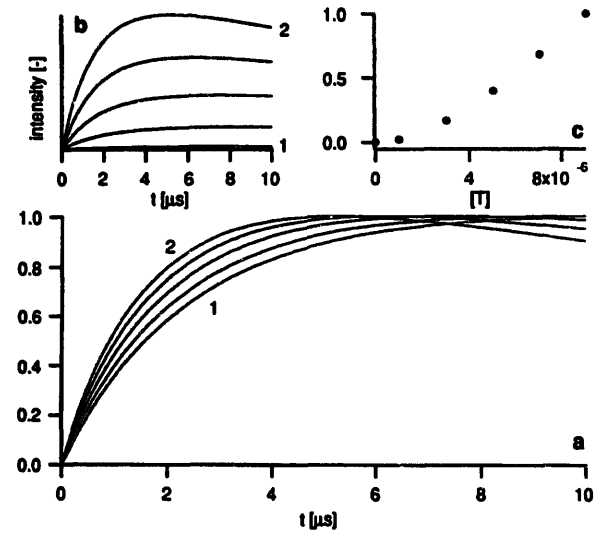

Fig. 7. (a) Normalized simulated TP kinetics; only TTA is the ion-forming process. The following values were taken: $k_0+k_Q[Q]=0.2\times10^6\ s^{-1}$, $k_{TT}=1.8\times10^{10}\ M^{-1}\ s^{-1}$, $k_{SQ}=0.5\times10^6\ M^{-1}\ s^{-1}$, $k_{rec}=2.0\times10^{10}\ M^{-1}\ s^{-1}$, $Pro_{TT}=1$, $Pro_{SQ}=0$, $[^1BP_0]=0.005$ M. The initial triplet concentration [T] was varied from 1×10^{-6} M (1) up to 9×10^{-6} M (2). (b) Non-normalized simulated TP kinetics. (c) Normalized simulated TP maxima plotted against the initial triplet concentration [T].

current rise if ions are only formed via this pathway (Eq. (3b2)). This effect is also reproduced by the simulations (Fig. 7).

Similar arguments can be put forward when the $^1BP_0$ concentration varies at the same laser pulse intensity. This situation implies that the triplet concentration also changes. If only SQ generates ions (Fig. 8), an increase in the absorbance results in a steeper rise of the photocurrent.

The variation of the absorbance plays no role in the photocurrent rise if only TTA generates ions and SQ has no effect. However, as the triplet concentration increases at higher absorbances, a similar effect to that shown in Fig. 7 is expected on the rise in the photocurrent. This rise should also be faster if a non-ionic process (Eq. (3c1)) deactivates ^3BP. In Fig. 9, a diffusion-controlled quenching reaction ($k_Q=2.0\times10^{10}\ M^{-1}\ s^{-1}$) is used for the simulation. This deactivation pathway applies to the traces recorded with different O_2 concentrations.

The rise of TP becomes steeper at higher O_2 concentrations, because of a new pathway which deactivates ^3BP through a non-ionic process. The oxygen effect is more pronounced in solutions of low $^1BP_0$ concentration, as can be seen from Fig. 5(a)–(c). At higher $^1BP_0$ concentrations, very little or no effect can be seen between the argon-bubbled and FPTS-degassed samples. This is understandable by considering the non-ionic deactivation pathways of ^3BP by oxygen quenching and SQ. In the $^1BP_0$ sample of lowest concentration (Fig. 5(a)), SQ is not so important; but with increasing $^1BP_0$ concentration (Fig. 5(b) and Fig. 5(c)), the SQ mechanism becomes increasingly important and finally overcomes the competitive pathway of the deactivation mechanism by oxygen.

The simulations tend to confirm the energetic considerations. Traces representing the ions generated by TTA in Fig. 7 agree most satisfactorily with the experimental kinetics. According to the simulations, ions generated by the SQ mechanism would be formed on a longer timescale (cf. Figs. 6–8).

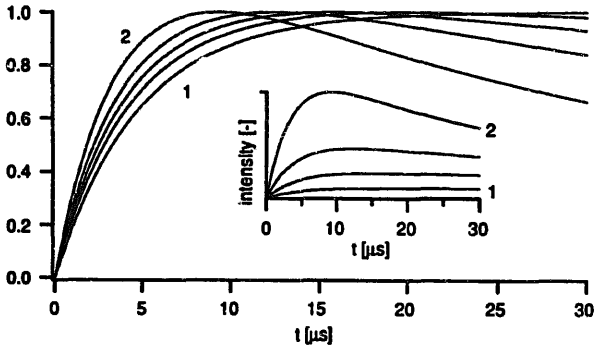

Fig. 8. Normalized and non-normalized (inset) simulated TP kinetics; only SQ is the ion-forming process. The following values were taken: $k_0+k_Q[Q]=0.2\times10^6\ s^{-1}$, $k_{TT}=1.8\times10^{10}\ M^{-1}\ s^{-1}$, $k_{SQ}=0.5\times10^6\ M^{-1}\ s^{-1}$, $k_{rec}=2.0\times10^{10}\ M^{-1}\ s^{-1}$, $Pro_{TT}=0$, $Pro_{SQ}=1$, $[^1BP_0]$ was varied from 0.001 M (1) up to 0.050 M (2). The corresponding initial triplet concentration [T] was adapted to the percentage of light absorbed by the sample, taking a value of 8×10^{-6} M at $[^1BP_0]=0.005$ M.

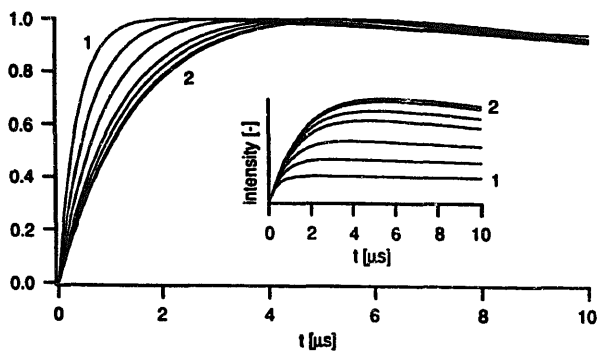

Fig. 9. Normalized and non-normalized (inset) simulated TP kinetics; only TTA is the ion-forming process; new non-ionic quenching process with Q. The following values were taken: $k_0=1\times10^4\ s^{-1}$, $k_{TT}=1.8\times10^{10}\ M^{-1}\ s^{-1}$, $k_{SQ}=0.5\times10^6\ M^{-1}\ s^{-1}$, $k_Q=2.0\times10^{10}\ M^{-1}\ s^{-1}$, $k_{rec}=2.0\times10^{10}\ M^{-1}\ s^{-1}$, $Pro_{TT}=1$, $Pro_{SQ}=0$, $[^1BP_0]=0.005$ M, $[T]=8\times10^{-6}$ M, [Q] was varied from 1.095×10^{-4} M (1) down to 9.5×10^{-6} M (2).

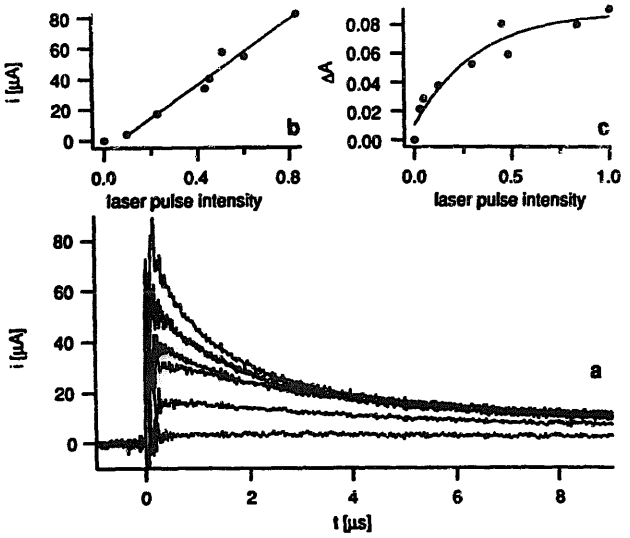

Fig. 10. (a) TP kinetics of BP ($[^1BP_0] = 8.5 \times 10^{-5}$ M, $A = 0.85$) in MeCN excited at 266 nm with different laser pulse intensities. (b) TP maxima plotted against the laser pulse intensity (the value of unity corresponds to an energy of 13 mJ per pulse). (c) ^3BP absorbance at 525 nm plotted against the laser pulse intensity. Strong saturation of the absorbance is observed with increasing laser pulse intensity.

3.2. Excitation at 266 nm

With 266 nm excitation, instantaneous current rises and much larger photocurrents are observed for a $^1BP_0$ concentration of 8.5×10^{-5} M ($A = 0.85$) (Fig. 10). The curves are in agreement with the work of Elisei et al. [4].

A plot of the laser pulse intensity against the observed signal yields a straight line which does not cross the origin (Fig. 10(b)). Normally, a monomolecular biphotonic process is expected to show a quadratic dependence on the excitation intensity. However, such a behaviour is a special case, only observed under well-defined conditions. Lachish et al. [18] simulated monomolecular biphotonic ionization processes and demonstrated that a linear relationship between the concentration of ionized molecules and the excitation intensity is possible. A 10 mJ pulse at 266 nm contains 1.34×10^{16} photons, but only 8.7×10^{15} molecules are present in the irradiated volume ($[^1BP_0] = 8.5 \times 10^{-5}$ M). Consequently, there are more photons than excitable molecules and Beer's law does not apply. The extinction coefficient of ^3BP at 266 nm is not known, but is probably not negligible. As confirmed in Fig. 10(c), the ^3BP concentration does not depend linearly on the excitation intensity. This explains why the observed TP maxima depend linearly on the laser pulse intensity. The ^3BP concentration of such a sample ($[^1BP_0] = 8.5 \times 10^{-5}$ M, $A = 0.85$), excited with a 10 mJ pulse, approximates to 1×10^{-5} M and TTA can also occur. However, the slower current contribution of TTA is masked by the larger current generated by the monomolecular two-photon ionization process.

4. Discussion

The change in the ion-generating mechanism with a shift in excitation from 355 nm to 266 mm is remarkable, because in addition to TTA a unimolecular biphotonic absorption process becomes operative. For the explanation of this alteration, it can be assumed that both processes involve the first triplet excited state T_1. The relaxation and intersystem crossing processes in BP are very fast and it is very improbable that a higher singlet state comes into play. Fig. 11 shows all the relevant energy states of BP in MeCN compared with the gas phase ionization potential of BP ($IP_v = 9.05$ eV [19]).

Solvation lowers the energy of the states by the dispersion term, which is assumed to be equal for all states and therefore will not be taken into consideration. For two-photon ionization, the second photon must be sufficiently energetic to reach the ionic state. Such a state would consist of $BP^{\cdot +}$ in contact with the solvated electron. This kind of transition should be considered as solute to solvent ET, rather than ionization, which relates to the gas phase. Due to the speed of the electronic transitions, the Franck–Condon principle can be applied and no stabilization through solvent relaxation can be gained. The dipole–induced dipole stabilization, which does not require solvent re-orientation, must be considered. This kind of stabilization can be estimated by applying Onsager's equation [20] ($E_{solv} = \mu^2/a^3 f(n^2)$, where μ is the dipole moment, a is the Onsager cavity radius and n is the refractive index (cgs units must be used)). Due to the lack of detailed structural information (e.g. radii of particles, charge localization), only a rough estimate can be made. Taking $\mu = 27$ D and the radii of $BP^{\cdot +}$ as 3.5 Å and $(MeCN)_2^{\cdot -}$ as 2.5 Å, the stabilization due to dipole–induced dipole interaction is approximately 2.5 eV (if $\mu = 15$ D, the stabilization energy is only 0.8 eV). Subtracting this solva-

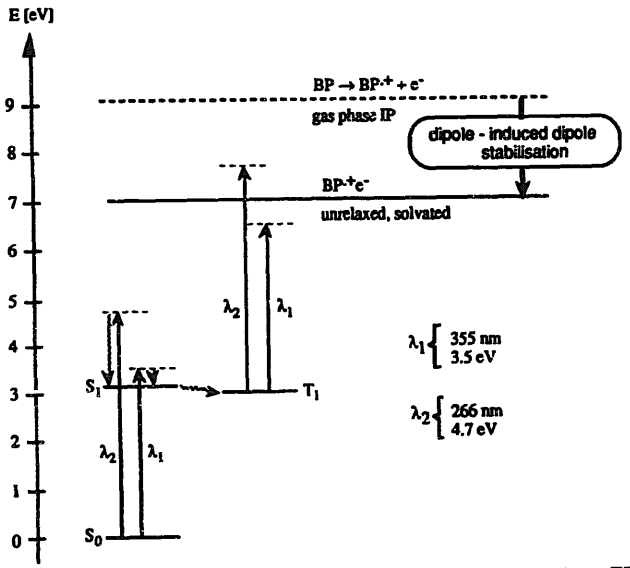

Fig. 11. State energy diagram of BP. The unrelaxed solute to solvent ET, calculated according to Onsager (see text), forms a threshold to the ionization mechanism.

tion energy from the ionization potential should yield a threshold line. Above this borderline, solute to solvent ET is possible, but below, relaxation to T_1 takes place and only TTA is operational.

The further development of tunable lasers will facilitate the scanning of the excitation wavelength and the determination of this threshold line. Clearly, TP is a sensitive detection technique which allows the determination of the energetics of ET reactions in liquid solvents.

Acknowledgements

This work was part of Project No. 2028-040398.94/1 of the Schweizerischer Nationalfonds zur Förderung der wissenschaftlichen Forschung. Thanks are due to E. Brosi for the construction of the TP cell and to P.-H. Chassot for the design of the single shot set-up.

References

[1] M.O. Delcourt, M.J. Rossi, J. Phys. Chem. 86 (1982) 3233.
[2] E. Vauthey, E. Haselbach, P. Suppan, Helv. Chim. Acta 70 (1987) 347.
[3] E. Vauthey, P. Suppan, E. Haselbach, R.S. Davidson, Helv. Chim. Acta 69 (1986) 430.
[4] F. Elisei, G. Favaro, H. Görner, J. Photochem. Photobiol. A: Chem. 59 (1991) 243.
[5] J.A. Ridick, W.B. Bunger, Organic Solvents, Wiley-Interscience, 1970.
[6] E. Hairer, S.P. Norsett, G. Wanner, Solving Ordinary Differential Equations I. Nonstiff Problems, Springer, 1993.
[7] H. Miyasaka, M. Kiri, K. Morita, N. Mataga, Y. Tanimoto, Bull. Chem. Soc. Jpn. 68 (1995) 1569.
[8] T.S. Fang, R. Fukuda, R.E. Brown, L.A. Singer, J. Phys. Chem. 82 (1978) 246.
[9] R.E. Brown, L.A. Singer, J.H. Parks, J. Am. Chem. Soc. 94 (24) (1972) 8584.
[10] M.W. Wolf, K.D. Legg, R.E. Brown, L.A. Singer, J.H. Parks, J. Am. Chem. Soc. 97 (16) (1975) 4490.
[11] M. von Raumer, P. Suppan, Chem. Phys. Lett. 250 (1996) 91.
[12] I.P. Bell, M.A.J. Rodgers, H.D. Burrows, J. Chem. Soc., Faraday Trans. 1 73 (2) (1977) 315.
[13] P. Suppan, J. Chem. Soc., Faraday Trans. 1 82 (1986) 509.
[14] R.O. Loutfy, R.O. Loutfy, J. Phys. Chem. 77 (3) (1973) 336.
[15] M.R. Rifi, F.H. Covitz, Introduction to Organic Electrochemistry, Dekker, 1974.
[16] L.A. Singer, R.E. Brown, G.A. Davis, J. Am. Chem. Soc., 95 (26) (1973) 8638.
[17] J.M. Harris, R.T. Camron, J. Phys. Chem. 97 (1993) 13 598.
[18] U. Lachish, A. Shafferman, G. Stein, J. Chem. Phys. 64 (10) (1976) 4205.
[19] G. Centineo, I. Fragala, G. Bruno, S. Spampinato, J. Mol. Struct. 44 (1978) 203.
[20] P. Suppan, J. Photochem. Photobiol. A: Chem. 50 (1990) 293.